# Forced folding and fracturing induced by differential compaction during post-depositional inflation of sandbodies: insights from numerical modelling

Qingfeng Meng*, David Hodgetts

*1. School of Earth and Environmental Sciences, University of Manchester, Manchester, M13 9PL, UK*

**Abstract**

Three series of numerical models based on the discrete element method were constructed to simulate forced folding and fracturing triggered by postdepositional inflation of fludised sandbody. The models consist of numerous particles that have relatively low to high interparticle bonds to represent overburden sediments with a relatively low to high cohesion, and cohesionless, frictionless particles to represent fluidised sands. The modelling results show that normal faults were produced due to the upward inflation of sand domes and the resulting flexed overburden, when the cohesion of the host sediments is low. Opening voids were created as a result of strata collapse, when the intrusion-related normal faults terminated within the host sediments as blind faults. Conical fractures that are aligned along sandbody margins were produced, which consist of closed, lower segments with a reverse displacement, and opening, middle-upper segments with a minor to zero shear component. Forced folds were generated in most models with a moderate to high cohesion, resulting in differential compaction in the overlying sediments that can account for the formation of fold-related fractures, which are either shear, hybrid or pure tensile, depending on their structural positions. The amplitude of forced folds is closely associated with both cohesion

* Corresponding author. E-mail address: meng.qingfeng@hotmail.com

and thickness of sediments in the overburden, whilst fold wavelength is mainly controlled by sediment cohesion. Based on the modelling results, three types of preferential sites for the storage of injected sands were suggested, which are believed to be instructive for subsurface sandbody detection and prediction. This study demonstrates that differential compaction induced by sand inflation can play an important role in overburden folding and fracturing.

**Key words:** forced fold; fracture; sandbody; sandstone intrusion; numerical modelling; discrete element

## 1. Introduction

Sandstone intrusions have been extensively studied with a long history of field-based research focused on meter-scale intrusive bodies (e.g. Diller, 1890; Jenkins, 1930; Peterson, 1966; Boehm and Moore, 2002; Huuse et al., 2005a; Hubbard et al., 2007; Vétel and Cartwright, 2010; Hurst et al., 2011; Moreau et al., 2012; Scott et al., 2013; Palladino et al., 2016, 2018; among many others). The study on large-scale sandstone intrusions has become increasing common in the past two decades using high-resolution three-dimensional seismic data from basins where such structures are developed (e.g. Molyneux et al., 2002; Hurst et al., 2003a; Hurst et al., 2003b; Cartwright and Huuse, 2005; Davies et al., 2006; Cartwright, 2007; Cartwright et al., 2007; Huuse et al., 2005b, 2007, 2010; Lonergan et al., 2007; Vigorito et al., 2008; Jackson et al., 2011). Understanding the mechanisms of sandstone intrusions is critically important, not only because that they can significant influence reservoir architecture (Fig. 1) and connectivity, reservoir volumetrics and pore-scale reservoir properties (Lonergan et al., 2000) and thereby affect hydrocarbon exploration and production from those reservoirs (Huuse et al., 2003; de Boer et al., 2007; Hurst and Cartwright, 2007; Hurst et al., 2006, 2007, 2016; Hurst and Vigorito, 2017), but also because of their crucial role in understanding petroleum systems and basin evolution in general (Cartwright, 2010).

The geometric variability and distribution of subsurface sandstone intrusions can be extremely complex and be difficult to map because they are commonly at or below seismic resolution (Jackson et al., 2007). Many researchers have attempted to develop conceptual models of sand-intrusion processes and the associated deformations in the overburden, shedding light on channel surface geometries (Lonergan et al., 2000), development of forced folds (Cosgrove and Hillier, 1999; Shoulders and Cartwright, 2004; Frey-Martnez et al., 2007; Szarawarska et al., 2010), formation and propagation of intrusion-related faults/fractures in the overlying sediments (Rodrigues et al., 2009; Mourgues et al., 2012; Bureau et al., 2014; Haug et al., 2018), and interactions of sand intrusions with pre-existing structures (Lonergan and Cartwright, 1999; Molyneux et al., 2002; Shoulders et al., 2007; Bureau et al., 2013; Løseth et al., 2013). In particular, sandstone intrusions that occur in a conical form (Molyneux et al., 2002; Huuse et al., 2005a; Jackson et al., 2007; Shoulders et al., 2007; Cartwright et al., 2008; Jackson et al., 2011), or referred to as wings (Huuse et al., 2004), have received great attention, however, their formation mechanics still remains controversial. Although sandstone intrusions have been more commonly suggested as hydraulic fractures, it has been realized that differential compaction induced by sandbody inflation may have played an important role in the formation of some dykes and sills, especially some peripheral dykes (Cosgrove and Hillier, 2000; Huuse et al., 2004). This is often evident from the domal or irregular sandbody surfaces and the flexed overburden (Lonergan et al., 2000; Frey-Martinez et al., 2007; Cartwright et al., 2008; Jackson et al., 2011) or the 'jack-up' phenomenon (Szarawarska et al., 2010).

This paper reports the modelling results of overburden deformation induced by inflation of fludised sandbody using the discrete element method. The aims of this paper are (1) to produce various types of structures that are associated with sandstone inflation and are comparable to those observed in nature; (2) to investigate the role of sediment cohesion and thickness in the development of forced fold; and (3) to better understand the formation mechanisms of dyke-sill complexes associated with postdepositional sandbody activities, especially those occurring in a mixed shear-extensional mode. The models presented provide new insights into the development and controls on forced folding and fracturing during sandstone inflation, and are believed to be applicable for the detection and prediction of subsurface sandstone injectites.

## 2. Methodology

### 2.1. Fundamental principles

The discrete element modelling method, based on elastic interactions between frictional rigid particles, was first developed by Cundall and Strack (1979) to simulate behavior and interaction of granular materials. The modelled materials consist of numerous elastic particles that displace independently from one another, and interact with neighbouring particles only at contacts between particles. Particle contact is defined as a linear spring in compression that resist particle overlap, and a frictional strength that resists shear motion (Fig. 2a). More complex behavior of a particle assembly can be simulated by allowing the particles to be bonded together so as to resist both shear and extensional displacements. The bonds will be broken once the bond strength is exceeded, which indicates the generation of microfractures. Coalescence of microfractures can subsequently result in larger macro sized fractures.

The mechanical behavior of a particle assembly is characterised by the movement of each particle and inter-particle forces acting on their contacts, which is governed by the force-displacement law. For dynamic calculations, the discrete element models follow an iterative, timestepping procedure that consists of repeated update of particle positions and inter-particle forces at each timestep (Cundall and Strack, 1999). This makes it possible to simulate the non-linear interaction of a series of particles.

Due to the particle-based nature, the discrete element model can produce realistic faults and fractures with a finite displacement. This method has been thereby widely used for modelling structural deformations across a wide range of scales, especially for modelling development of detachment fold (Hardy and Finch, 2005; Vidal-Royo et al., 2011; Meng and Hodgetts, 2019), fault-bend fold (Benesh et al., 2007), fault-propagation fold (Finch et al., 2003, 2004; Cardozo et al., 2005; Hardy and Finch, 2006, 2007; Hughes et al., 2014; Meng and Hodgetts, 2019) and faults/fractures (e.g. Schöpfer et al., 2006, 2007, 2011, 2016, 2017; Abe et al., 2011; Hardy, 2013; Spence and Finch, 2014; Virgo et al., 2013, 2014, 2016; Finch and Gawthorpe, 2017). The extensive applications of discrete element modelling to structural geology research make it an ideal method for addressing questions related to the present study.

### 2.2. Model configuration

Our discrete element models, constructed using the Particle Flow Code (Cundal and Strack, 1999), consist of a 2 km long rectangular box that has a two vertical side walls, a basal floor and an open top (Fig. 2b). The box is filled with numerous closely-packed, bonded particles with radii ranging from 1.0 to 3.2 m, to represent overlying sediments in the overburden. A 0.2 km high, right-angled equilateral triangle, located below the central part of the rectangular box, is filled with 18,516 non-bonded particles with radii ranging from 0.5 to 1 m, to represent fluidized sands. Notably, the geometry of the sandbody is highly simplified, and the aim of such a geometry is to allow the particles within the sandbody to radially spread upwards. Particle sizes in both the sandbody and the overburden follow a Gaussian distribution, which can help avoid hexagonal close packing of particles.

The particle stiffness is assigned with a value of 1e7 N/m for both normal (kn) and shear (Ks) stiffness, which are appropriate values for sandstones and correspond to a Young's Modulus of approximately 5 MPa for the bulk rock mass (Liu and Konietzky, 2018). Friction coefficient μ of particles in the overburden is assigned with a value of 0.25, whilst μ for particles in the sandbody is set to zero. The particle density ρ is 2600 $kg/m^3$. The bonding cohesion for particles in the overburden is set to be between 1 to 8 MPa, to represent sediments with a relatively low to high cohesion.

The packing of particles was achieved by allowing an assembly of randomly-generated particles to settle to the bottom of the model under their own weight. The system was considered to have reached static equilibrium when the mean unbalanced force within the particle assembly have dropped to a negligible value. The particle assembly was then trimmed to the desired height, which led to a small amount of vertical elastic rebound and elevated the surface. We then repeated the trimming process that allowed the system to be settled. The particle assembly in the overburden was trimmed to a height of 0.28, 0.35 and 0.42 km, to represent a relatively thin to thick overburden respectively. The overburden sediments are mechanically homogeneous. Colours were assigned to the overburden sediments simply for bedding correlations.

The model boundaries are defined by elastic walls that share the same mechanical properties with their contacting particles. Deformation of the system was driven by a horizontal wall underneath the sandbody that moved upward at a constant rate of 0.5 m per timestep. This helps represent a lithostatic stress condition during sand fluidization and inflation. The models were gravitationally loaded by 1 g.

We mainly focused on the macroscopic deformations and structures generated as a result of sandbody inflation, especially on forced folds and faults/fractures. Only the models that exhibit realistic features are presented. The models that reproduced classical, widely reported structures were selected for a more detailed analysis, regarding their sequential deformation processes and evolving stress fields. By varying the cohesion and thickness of particles in the overburden, we also made an evaluation of their control on the development and patterns of inflation-related structures.

## 3. Results

### 3.1. Modelling results

#### 3.1.1. Series 1: models 1-4

Models 1-4 with a relatively thin overburden exhibited varied deformation patterns in the overburden. Model 1 produced multiple normal faults in the layers above the sandbody (Fig. 3a). Two faults (F1 and F2) propagated to the surface as through-going faults, and created fault scarps in the uppermost layer during normal slipping. F1 and F3, which are dipping towards opposite directions, constitute a small horst located above a symmetrical sand dome. F2 and F4 occur along the margins of the sandbody, with the fault-bounded blocks acting as footwalls.

Model 2 produced multiple small normal blind faults in the sediments below the magenta layer (Fig. 3b). These faults correspond to the concaves and convexes on the irregular sandbody surface. Notably, a forced fold was formed in the overburden. An opening-mode fracture was generated in the fold hinge, where the layers exhibit the maximum curvature. This fracture propagated downwards to the magenta layer and exhibits a downward tapering tip.

Similar to model 2, model 3 produced a force fold and an opening-mode fracture that reached downwards to the orange layer (Fig. 3c). Below the orange layer, a minor normal fault was developed due to the cone-shaped sand intrusion that uplifted the sediments in the footwall. The other parts of the forced fold are smoothly curved.

Model 4 produced a force fold in the overlying sediments of the sandbody, however, the overburden remained intact with no faults being formed (Fig. 3d). The layers are smoothly curved and parallel to the upper sandbody surface.

**3.1.2. Series 2: models 5-10**

The modelling result of model 5 is rather similar to that of model 1, regarding fault patterns and sandbody surface geometry. Model 5 produced multiple normal faults that transect the sediments above the sandbody (Fig. 4a), with fault scarps being created on the surface. A sand dome with a rounded top protruded into the overlying sediments, with a through-going faults developed along its right flank. Normal faults are also developed along the margins of the sandbody.

Model 6 produced two normal faults in the sediments above the sandbody, and a cone-shaped sand protrusion with a sharp top (Fig. 4b). The two normal faults define a small horst above the sand protrusion. One of the faults is a through-going fault developed along the flank of sand protrusion. Two opening voids were created during fault slip due to the irregularities on the fault surface. The sandbody exhibits an asymmetric geometry, and its surface remains largely planar.

Model 7 produced two minor blind normal faults that cut layers between the sandbody and the magenta layer (Fig. 4c). These two faults define a minor horst that was formed due to the uplift of the sediments by sand protrusion. Interestingly, a void was created between the gray layer and the magenta layer, where the two faults intersect, due to strata collapse. The sandbody surface is largely planar except the concave segment on the right of the fault that allowed accommodation of the sediments in the hanging-wall.

A graben side-by-side with two horsts was formed in model 8, which is bounded by two minor normal faults (Fig. 4d). Two opening voids were created where faults intersect, because of strata collapse in the hangingwalls of the normal faults, similar to model 7. The sandbody surface exhibits a concave, with two faults developed along its flanks. The concave accommodated sediments in the graben.

Model 9 produced a normal fault that occurs along the left flank of a cone-shaped sand protrusion, and reached the red layer (Fig. 4e). The fracture tip can be subdivided into a hybrid-mode, inclined segment, and an opening-mode sub-vertical segment. Notably, the inclined segment is aligned normal to the surface of the surface of the underlying sandbody.

Model 10 produced a rather symmetric forced fold in the overburden (Fig. 4f). Similar to model 4, the layers and the sandbody surface were smoothly curved and parallel with each other. No faults were formed in this model.

#### 3.1.3. Series 3: models 11-18

Model 11 produced a large horst with normal faults developed along the margins of the sandbody (Fig. 5a). The faults on the left of the sandbody are through-going faults, resulting in a fault scarp on the surface. The sandbody surface is relatively planar comparing to the other models.

Similar to model 11, model 12 also produced a horst in the sediments above the sandbody (Fig. 5b). Differently, the fault F2 passed into a reverse fault above the blue layer, resulting in a push-up structure on the surface. Two parallel opening-mode fractures were generated due to the normal displacement of F1.

Model 13 produced two high-angle reverse faults in the overburden that resulted in a push-up structure on the surface, with two fault scarps being created (Fig. 5c). The sandbody surface exhibits a sub-rounded small dome in its center. The dome caused gentle folding of the beds below the magenta layer, whilst the upper layers were not influenced.

Model 14 produced three main faults, including an opening-mode fracture (F1) in the hinge of the forced fold, and a pair of oppositely dipping faults (F2 and F3) below the green layer (Fig. 5d). Both F2 and F3 have a closed, lower segment with a reverse displacement, and an upper segment occurring in an opening-mode. Interestingly, the opening, inclined segment of F2 passed into a sub-horizontal, purely opening-mode fracture towards its tapering tip.

The modelling results of models 15 and 16 are similar (Fig. 5e, f). Both models produced a normal fault F1 in the hinge of the forced fold with their upper segments occurring in a hybrid mode, and a reverse fault F2 passing into an opening fracture. Similar to model 14, the opening segment of F2 of model 16 also consist of a sub-horizontal, tapering tip that occurs in a pure opening mode.

Model 17 produced two main faults in the overburden, including one in the fold hinge and the other as a hybrid fracture developed along the sandbody margin (Fig. 5g). Differently from previous two models, F1 in the fold hinge exhibits a reverse displacement. Notably, the opening segments of F2 consists of steep en echelon fractures and horizontal steps that link neighbouring steep fractures.

Model 18 only generated one opening fracture, with a reverse sense of shear, in the hinge of the force fold (Fig. 5h). The layers are smoothly curved, without additional fractures being produced to cut the overburden.

### 3.2. Syn-intrusion deformation and stress field in the overburden

Two models (5 and 14) that appear to be the most compatible with natural observations of sandstone intrusions regarding injectite geometry and fault/ fracture patterns, were selected for a more detailed analysis of the entire intrusion process and syn-intrusion deformations in the overburden.

### 3.2.1. Model 5

Model 5 produced an array of normal faults in the overburden, with distinguishable normal displacement and fault scarps, and a rather symmetric dome on the sandbody surface (Figs 4a and 6). Initially (T1), the overburden remained intact whilst a small amount of sands were intruded into the overlying layers (Fig. 4a). This led to concentration of horizontal tensile stresses in the upper layers of the overburden (Fig. 4b). Later (T2), a minor dome was formed in the central part of the sandbody, resulting in differential compactions of the upper gray and orange layers and the subsequent formation of a minor blind normal fault. The stress field was dominated by compressive stresses in the surrounding area of the injectites, whilst horizontal tensile stresses were increasingly intensive in the uppermost layers of the overburden above the sandbody. At T3, the dome continued to grow with an increasing dome height. The minor fault propagated upward to the magenta layer. The stress field is similar to that at the earlier stages, only more intensified of the tensile stresses in the upper layers. After that (T4), a through-going normal fault was formed that transected the entire overburden, with an opening fault scarp being developed on the overburden surface. Meanwhile, minor normal faults with oppositely-dipping directions were generated at the sandbody margins. The extent of tensile stress distribution became narrower than the previous stage. In particular, tensile stresses were dropped dramatically in the fault zones. At T5, F2, that is parallel to F1, propagated to the overburden surface as a through-going fault. This was accompanied with a decreased extent of the horizontal tensile stresses to be in the hangingwall rocks of F2 right above the sandbody. At the final stage, both the width and height of the dome increased, leading to increased fault displacement of all faults in the overburden. The system exhibits a pattern similar to a half graben. The stress field is similar to that at T5.

### 3.2.2. Model 14

Model 14 produced a pair of oppositely-dipping, opening mode fractures in the overburden (Figs 5d and 7). Initially (T1), although the intrusion of the sandbody sands did not cause distinguishable deformation in the overburden (Fig. 7a), it gave rise to the development of tensile stress concentrations located in the upmost layers above the channel (Fig. 7b). At the following stage (T2), the sandbody exhibited a domal surface, which is smoothly curved across the entire surface. The tensile stresses became more intensified, and the stress trajectories were aligned in a half-circular manner above the sandbody. At T3, a vertical opening-mode fracture was formed, accompanied with a dramatic drop of tensile stress in the uppermost layers. Later (T4), a pair of conical, opening-mode fractures were formed where tensile stresses were concentrated. Tensile stresses were concentrated in the tip regions of the opening-mode fractures. At T5, the size of both conical fractures increased significantly. The left fracture propagated upwards by the linkage of several sub-parallel en echelon fractures and their sub-horizontal steps. The opening segments of the conical fractures did not exhibit relative displacement of fracture walls, whilst the lower segments of the fractures were closed and exhibited a reverse displacement. At the final stage (T6), the left fracture, with a horizontal fracture tip, reached the red layer. Aperture of all the three opening fractures were increased. The distribution of tensile stresses was similar to the previous stages (T4 and T5), i.e. the tensile stresses were mainly localized within fracture tip regions and adjacent areas.

### 3.3. Surface deformation

Most of the models presented produced forced folding of the overburden due to the intrusion of sandbody sands, except model 5. Here, we focus on the forced folding of the surface layer, regarding the fold amplitude and wavelength that are represented by the maximum surface uplift and width of the uplifted domain respectively. Fig. 8 shows the plot of overburden rock cohesion versus the maximum surface uplift and width of the uplifted domain, to reveal their relationships. It is demonstrated that, in general, a higher cohesion of the overburden rocks can result in a greater surface uplift, and a greater width as well, although exceptions occur. The greatest surface uplift of 66.6 m occurs in model 10 that has the highest cohesion among model series 2. Model 18 that has the highest cohesion among all models, exhibits the greatest width of an uplifted domain of 1.22 km.

## 4. Discussion

### 4.1. Controls on forced folding of the overburden

Intrusion-related, forced folds have been commonly found to develop above sandstone intrusions with domal surfaces (Nichols, 1995; Frey-Martnez et al., 2007; Hamberg et al., 2007; Szarawarska et al., 2010), in a manner analogous with forced folding induced by igneous intrusions (e.g. Hansen and Cartwright, 2006; Hansen et al., 2008; Jackson et al., 2013; Omosanya et al., 2017). Forced folding occurs in the sedimentary cover overlying remobilised sand bodies during their mechanical emplacement, in order to compensate for the added thickness provided by the intruded sands

(Hansen et al., 2008). Forced folds are, thereby, regarded as a diagnostic feature of an intrusive origin (Szarawarska et al., 2010). Forced folds are of great importance for both depositional and structural analysis. Forced folds associated with sand intrusions may control the thickness and stratal architecture of subsequently deposited units (Frey-Martnez et al., 2007; Huuse et al., 2007; Cartwright et al., 2008). Moreover, onlap onto the flanks of forced folds allows dating of the intrusions (Shoulders and Cartwright, 2004; Shoulders et al., 2007). Although forced folds that are accompanied with sandstone intrusions have received increasing attention, the controls on the fold geometries, aside from the volume of intruded sands, are difficult to be determined, due to the lack of comparisons of forced folds developed in different geological contexts. A recent study has suggested that, for igneous intrusions, the cohesion of sedimentary covers could control the geometry of forced folds and the aspect ratios of intrusive bodies as revealed by sandbox experiments (Schmiedel et al., 2017).

Here, our models can help address this issue by varying the value of one parameter whilst the others being kept constant. It is demonstrated in the modelling results that both the cover rock cohesion and overburden thickness are crucial controlling factors for forced folds (Fig. 8). The cover rock cohesion exhibits a positive correlation to the size of forced fold, i.e. the higher the cohesion is, the greater the fold amplitude and wavelength are. Forced fold may not be formed during forceful injection of sands, if the intrusion timing is early and the cover sediments has a very low cohesion, i.e. a low degree of lithification. With the same cover rock cohesion, the forced folds predominantly exhibit a lower amplitude when the overburden is thicker. The relationship between the wavelength of forced folds and fold amplitude is unclear for models with the same cover rock cohesion, indicating that fold wavelength is more intimately associated with cover rock cohesion, whilst overburden thickness may play a much less important role in controlling wavelength of forced folds.

It should be noted that some other factors that were not considered in this study, can also influence the geometry and size of forced folds, including stiffness of the cover sediments, variations of mechanical properties across the sedimentary successions (i.e. mechanical stratigraphy), and spatial variations of those factors.

## 4.2. Faulting and fracturing mechanisms

### 4.2.1. Failure mode

Generally, sandstone intrusions are regarded as opening-mode, natural hydraulic fractures that occur when fluid pressure within remobilised sands exceeds the sum of the minimum principal stress and tensile strength of the host rock (Cosgrove, 2001; Jolly and Lonergan, 2002; Cartwright et al., 2008; Cartwright, 2010). Remobilised materials can then exploit these faults/fractures as transport pathways due to the fact that they are the mechanically easier option (Weertman, 1980; Donnadieu and Merle, 1998). However, the structural response of the flexed overburden during the early stage of sand inflation, especially prior to overpressure, has been largely ignored.

The modelling results presented demonstrate that shear, tensile and hybrid fault/fractures (both normal and reverse) can be induced in the overburden by inflation of sandbodies and forceful intrusion of sands into the overlying sediments. These fault/fractures are predominantly fold-related, due to differential compaction in the adjacent sediments during progressive fold development, which largely agrees with Cosgrove and Hillier (1999).

The fold-related faults/fractures can be subdivided into three main types, including 1) normal (Figs 3a-b, 4a-e, 5a-b,) and reverse faults (Fig. 5b-g) that correspond to the irregularities of the sandbody surface, and also along sandbody margins; 2) inclined or sub-horizontal pure tensile fractures aligned along the channel margins, and are not directly connected to the sandbody (Fig. 5d-g); and 3) pure tensile, or hybrid subvertical, downward propagating fractures in the hinge zones of the forced fold (Figs 3b-c, 5d-h).

Faults/fractures of type I can be attributed to differential compaction induced by the intrusive bodies, and their formation mechanism is further discussed in the following section. Faults/fractures of type II have been commonly observed in seismic data as dyke-sill complexes, and are referred to as winglike structures (Huuse et al., 2007; Jackson et al., 2007; Jackson et al., 2011; Jackson and Sømme, 2011). Fault/fractures of type III have been reported to be associated with intrusions (Cosgrove and Hillier, 1999; Hansen and Cartwright, 2006; Mathieu et al., 2008), as the result of curvature-related stretching and subsequent tensile fracturing in the hinge zones of intrusion-induced force folds. It is, therefore, believed that the three series of models have successfully reproduced many characteristic features of sandstone intrusion-related folds and faults/fractures.

**4.2.2. Intrusion-induced normal faults vs. pre-existing polygonal faults**

It has been recognised that normal faulting can be triggered by sandstone intrusions as a result of gravitational collapse off sand domes (Dixon et al., 1995; Palladino, et al., 2018). The intrusion-related normal faults have been suggested to have dramatically modified the geometries of the depositional sand bodies, and influenced formation and propagation of sand dykes and sill complexes in the Late Paleocene and Early Eocene submarine sandstone reservoirs in the Bruce-Beryl Embayment, northern North Sea (Dixon et al., 1995), Eocene Alba Field, UKCS (Cosgrove and Hiller, 2000) and also in central California (Palladino, et al., 2018). Our models with a low cover rock cohesion and a thin to intermediate overburden thickness, i.e. models 1, 5 and 6, largely agree to this explanation. Moreover, our models well illustrate the relationship between the development of sand domes and nucleation and propagation of normal faults (Fig. 6).

Polygonal faults (Fig. 9), occurring as networks of early diagenetically induced shear failure of fine-grained sediments (Cartwright, 1994, 2011; Cartwright and Lonergan, 1996; Goulty, 2008; Davies et al., 2009), have been frequently found to coexist with sandstone intrusions in the North Sea (Huuse et al., 2004; Huuse and Mickelson, 2004; Jackson et al., 2007, 2011; Shoulders et al., 2007; Szarawarska et al., 2010). It has been suggested that the pre-existing normal faults may have facilitated sandstone remobilisations and injections along dilated polygonal fault planes (Lonergan and Cartwright, 1999; Molyneux et al., 2002). However, some intrusions have been observed not to be affected by polygonal faults (Bureau et al., 2013). Moreover, the normal faults were found to be predominantly steeper than polygonal faults (Shoulders et al., 2007), indicating that not all the normal faults within sand intrusion-bearing layers can be simply interpreted as pre-existing polygonal faults.

Our modelling results help verify that normal faults can be formed as a result of sandstone intrusion (Figs 3a-b, 4a-e, 5a-b), due to differential compaction in the overlying sediments caused by sand doming, especially when the sediment cohesion is low, i.e. the timing of sand intrusion is early.

This can help explain the origin of some normal faults developed in the sediments overlying the sandbody. It is likely that many normal faults could result from differential compaction during the development of irregular sandbody surfaces as they intrude upwards. The sediments on the footwalls may experience more uplift by sand domes (or mounds), causing relative motions of sediments on different sides of the domes and subsequent normal faulting. Notably, due to the early timing of intrusion, the overlying sediments were not fully consolidated, allowing a localized intrusion-related compaction of those sediments, without causing a volumetric expansion. Hence, surface uplift or significant forced folding would not occur under such conditions (Figs 3a and 4a).

### 4.2.3. Dyke-sill complex

It has been reported that sandstone intrusions commonly consist of inclined dykes and subhorizontal sills (Jackson et al., 2011). Dykes are commonly observed to be aligned along sandbody margins and were described as winglike structures (Huuse et al., 2004; Jackson et al., 2011). Sills serve either as frontmost tips of injectites passed from upward propagating dykes, or as steps that link adjacent dykes (Lonergan et al., 2000; Jackson et al., 2011). Models 14-17 well reproduced fault/fracture systems that resemble the dyke-sill complexes described in previous studies.

The winglike dykes developed along margins of remobilised channels have been suggested to occur as peripheral dykes (Cosgrove and Hillier, 1999) due to different strains within a flexed overburden above intrusive bodies (Pollard and Johnson, 1973). However, our modelling results suggests that differential compaction would lead to nucleation and upward propagation of reverse faults along sandbody margins rather than pure opening-mode, upward-tapering fractures (Fig. 5d-g). The reverse faults passed into opening-mode fractures as they propagated upwards, either in a hybrid mode or in a pure tensile mode. The reverse sense of shear becomes neglectable in the tips of those opening-mode fractures (Fig. 5f).

Models 14 and 17 demonstrate the development of sub-horizontal sills that link neighbouring dykes. Those sills were generated as dilational jogs in the tip overlapping zones of dykes during their propagation, which is evident from both field (Jolly and Lonergan, 2002) and seismic observations (Jackson et al., 2011). Alternative explanations of sills in dyke-sill complexes were attributed to local stress variations or pre-existing mechanical weaknesses, such as bedding (Pollard and Johnson, 1973; Boehm and Moore, 2002; Kavanagh et al., 2006; Cartwright et al., 2008; Menand, 2008) or unconformity (Huuse et al., 2004). However, our models 14, 16 and 17 produced sub-horizontal opening fractures as the frontmost tip of the intrusion-induced fractures in a homogenous media (Fig. 5). Such fractures can serve as preferential sites for subsequent storage of remobilised sands, and evolve into sills. It is, therefore, argued that the formation of sib-horizontal sills, especially the frontmost segments of winglike structures, may not result from either local stress variations, or mechanical heterogeneities, such as bedding. Instead, they may be produced by tensile stresses originated as a result of the uplift of the overlying sediments of remobilised sands. Notably, this can only be possible when the sediments have a cohesion high enough to prevent gravitational collapse and fracture healing.

### 4.3. Implications for the storage of injected sands

Due to the complexity of sand injectites and the insufficient seismic resolution in mapping steeply dipping sand units, it can be problematic to characterise the geometry, size and distribution of subsurface sand injectites, especially the sub-seismic injectites (Jackson et al., 2007). Nevertheless, our modelling results provide new insights for predicting preferential sites for the storage of sand injectites. Such sites mainly include: 1) opening voids created along irregular surfaces of intrusion-induced faults during fault slip (Fig. 4b); 2) opening spaces created on top of grabens due to strata collapse (Fig. 4c-e); and 3) middle-upper segments of conical fractures that are aligned along sandbody margins (Fig. 5d-g). These sites provide opening spaces that can preferentially accommodate fluidised sands when the sands enter these sites and fluid pressure is dropped to be insufficient to jack up shear fractures.

It is possible that the winglike dykes may not emanate from sandbody margins as previous suggested, due to the prevalent compressive stresses that dominant the areas adjacent to the remobilised sands (Fig. 7b). The reverse faults that are attached to the sandbody can be dilated and serve as transport pathways for fluidized sands, however, they may be closed when fluid pressure drops, and thereby not favour sand storage. Differently, the intrusion-related fractures may occur in an opening mode in their middle to upper segments, and can accommodate injected sands that migrate along the fractures and enter these parts. Fig. 10 shows a field example of remobilised sands with a steeply-dipping wing sheet in the Triassic marls of the Mercia Mudstone Group, Somerset, SW England, which can help verify the point made above. The wing sheet exhibits clear thickness variations along its propagation direction. The lower segment of the wing exhibits a downward tapering tip, and is not directly connected to the sub-horizontal basal sandbody in the 2D section. The wing sheet shares the same grain size and mineral composition with the basal sandbody, and has been suggested to be sand injectites sourced from the basal sandbody during its remobilisation (Meng et al., 2017). The geometry of this sand wing and the spatial relationships between the wing and its source sandbody demonstrate that sand wings resulted from sand remobilisations may not in all cases directly emanate from sandbody margins, and that the faulted areas adjacent to remobilised sands may not be consistently open throughout the entire sand remobolisation and favour sand storage.

It is worth mentioning that the models presented are highly simplified, without aiming to directly simulate any specific natural prototypes. The main limitations of our models are that the roles of fluid pressure, mechanical stratigraphy and sandbody geometry were not considered. It is, therefore, suggested that future studies can incorporate these factors, especially for specific case studies with regional and local geological contexts being provided.

## 5. Conclusions

This study utilized the discrete element modelling method to simulate overburden forced folding and fracturing induced by inflation of fludised sandbodies. We conclude the following:

(1) Inflation of fludised sands can trigger normal faulting of the overburden when the host sediments have a low cohesion, i.e. a low level of lithification. The formation of normal faults can be attributed to sand doming-induced differential compaction in the overlying sediments.

(2) Sandstone inflation can result in forced folding of the overlying, cemented sediments and thereby a flexed overburden. Differential compaction across the inflated sandbody can produce faults/fractures along channel margins and also in fold hinge zones.

(3) The modelling results demonstrate a positive correlation between the cohesion of the overlying sediments and the amplitude and wavelength of the forced fold, i.e. the higher the cohesion is, the greater the amplitude and wavelength of the force fold are. With the same cover rock cohesion, the forced fold will exhibit a lower amplitude if the overburden is thicker. The overburden thickness does not play an important role in controlling the wavelength of the forced fold.

(4) The differential compaction induced by sandstone inflation can result in conical, opening fractures that consist of both steep and subhorizontal segments. The formation of sub-horizontal opening fractures may not necessarily be attributed to local stress variations or mechanical heterogeneities in the overburden, but could result from tensile stresses developed due to uplift of the overlying sediments above remobilised channels. Such fractures could evolve into dyke-sill complexes when fluidized sands entered these fractures.

(5) Our modelling results suggest that opening spaces that favour the storage of remobilised sands mainly include 1) voids created along faults with irregular, rough fault planes; 2) opening spaces created above intrusion-induced grabens; and 3) middle-upper opening segments of conical faults/fractures that are aligned along channel margins.

**Acknowledgements**

This work was supported by the Sandstone Injection Research Group (SIRG) consortium. Itasca is thanked for technical support. We thank Mads Huuse and Andrew Hurst for beneficial suggestions.

## References

Abe, S., Van Gent, H., Urai, J.L., 2011. DEM simulation of normal faults in cohesive materials. Tectonophysics 512, 12-21.

Benesh, N.P., Plesch, A., Shaw, J.H., Frost, E.K., 2007. Investigation of growth fault bend folding using discrete element modeling: Implications for signatures of active folding above blind thrust faults. Journal of Geophysical Research: Solid Earth 112, B03S04, doi:10.1029/2006JB004466.

Boehm, A., Moore, J.C., 2002. Fluidized sandstone intrusions as an indicator of paleostress orientation, Santa Cruz, California. Geofluids 2, 147-161.

Bureau, D., Mourgues, R., Cartwright, J., 2014. Use of a new artificial cohesive material for physical modelling: Application to sandstone intrusions and associated fracture networks. Journal of Structural Geology 66, 223-236.

Bureau, D., Mourgues, R., Cartwright, J., Foschi, M., Abdelmalak, M.M., 2013. Characterisation of interactions between a pre-existing polygonal fault system and sandstone intrusions and the determination of paleo-stresses in the Faroe-Shetland basin. Journal of Structural Geology 46, 186-199.

Cardozo, N., Allmendinger, R.W., Morgan, J.K., 2005. Influence of mechanical stratigraphy and initial stress state on the formation of two fault propagation folds. Journal of Structural Geology 27, 1954-1972.

Cartwright, J.A., 1994. Episodic basin-wide fluid expulsion from geopressured shale sequences in the North Sea basin. Geology 22, 447-450.

Cartwright, J.A., Lonergan, L., 1996. Volumetric contraction during the compaction of mudrocks: a mechanism for the development of regional-scale polygonal fault systems. Basin Research 8, 183-193.

Cartwright, J., Huuse, M., 2005. 3D seismic technology: the geological 'Hubble'. Basin Research 17, 1-20.

Cartwright, J., 2007. The impact of 3D seismic data on the understanding of compaction, fluid flow and diagenesis in sedimentary basins. Journal of the Geological Society 164, 881-893.

Cartwright, J., Huuse, M., Aplin, A., 2007. Seal bypass systems. AAPG Bulletin 91, 1141-1166.

Cartwright, J., James, D., Huuse, M., Vetel, W., Hurst, A., 2008. The geometry and emplacement of conical sandstone intrusions. Journal of Structural Geology 30, 854-867.

Cartwright, J., 2010. Regionally extensive emplacement of sandstone intrusions: a brief review. Basin Research 22, 502-516.

Cartwright, J., 2011. Diagenetically induced shear failure of fine-grained sediments and the development of polygonal fault systems. Marine and Petroleum Geology 28, 1593-1610.

Cosgrove, J.W., Hillier, R.D., 1999. Forced-fold development within Tertiary sediments of the Alba Field, UKCS: evidence of differential compaction and post-depositional sandstone remobilization. Geological Society, London, Special Publications 169, 61-71.

Cosgrove, J.W., 2001. Hydraulic fracturing during the formation and deformation of a basin: A factor in the dewatering of low-permeability sediments. AAPG Bulletin 85, 737-748.

Cundall, P.A., Strack, O.D.L., 1979. A discrete numerical model for granular assemblies. Geotechnique 29, 47-65.

Cundall, P.A., Strack, O.D.L., 1999. Particle flow code in 2 dimensions. Itasca consulting group, Inc.

Davies, R.J., Huuse, M., Hirst, P., Cartwright, J., Yang, Y., 2006. Giant clastic intrusions primed by silica diagenesis. Geology 34, 917-920.

Davies, R.J., Ireland, M.T., Cartwright, J.A., 2009. Differential compaction due to the irregular topology of a diagenetic reaction boundary: a new mechanism for the formation of polygonal faults. Basin Research 21, 354-359.

de Boer, W., Rawlinson, P.B., Hurst, A., 2007. Successful exploration of a sand injectite complex: Hamsun prospect, Norway Block 24/9. AAPG Memoir 87, 65-68.

Diller, J.S., 1890. Sandstone dikes. Bulletin of the Geological Society of America 1, 411-442.

Dixon, R.J., Schofield, K., Anderton, R., Reynolds, A.D., Alexander, R.W.S., Williams, M.C., Davies, K.G., 1995. Sandstone diapirism and clastic intrusion in the Tertiary submarine fans of the Bruce-Beryl Embayment, Quadrant 9, UKCS. Geological Society, London, Special Publications 94, 77-94.

Donnadieu, F., Merle, O., 1998. Experiments on the indentation process during cryptodome intrusions: New insights into Mount St. Helens deformation. Geology 26, 79-82.

Finch, E., Hardy, S., Gawthorpe, R., 2003. Discrete element modelling of contractional fault-propagation folding above rigid basement fault blocks. Journal of Structural Geology 25, 515-528.

Finch, E., Hardy, S., Gawthorpe, R., 2004. Discrete-element modelling of extensional fault-propagation folding above rigid basement fault blocks. Basin Research 16, 467-488.

Finch, E., Gawthorpe, R., 2017. Growth and interaction of normal faults and fault network evolution in rifts: insights from three-dimensional discrete element modelling. Geological Society, London, Special Publications 439, https://doi.org/10.1144/SP439.23.

Frey-Martnez, J., Cartwright, J., Hall, B., Huuse, M., 2007. Clastic intrusion at the base of deep-water sands: A trap-forming mechanism in the eastern Mediterranean. AAPG Memoir 87, 49-63.

Goulty, N.R., 2008. Geomechanics of polygonal fault systems: a review. Petroleum Geoscience 14, 389-397.

Hamberg, L., Jepsen, A.M., Ter Borch, N., Dam, G., Engkilde, M.K., Svendsen, J.B., 2007. Mounded structures of injected sandstones in deep-marine Paleocene reservoirs, Cecilie field, Denmark. AAPG Memoir 87, 69-79.

Hansen, D.M., Cartwright, J., 2006. The three-dimensional geometry and growth of forced folds above saucer-shaped igneous sills. Journal of Structural Geology 28, 1520-1535.

Hansen, D.M., Redfern, J., Federici, F., Di Biase, D., Bertozzi, G., 2008. Miocene igneous activity in the Northern Subbasin, offshore Senegal, NW Africa. Marine and Petroleum Geology 25, 1-15.

Hardy, S., Finch, E., 2005. Discrete-element modelling of detachment folding. Basin Research 17, 507-520.

Hardy, S., Finch, E., 2006. Discrete element modelling of the influence of cover strength on basement-involved fault-propagation folding. Tectonophysics 415, 225-238.

Hardy, S., Finch, E., 2007. Mechanical stratigraphy and the transition from trishear to kink-band fault-propagation fold forms above blind basement thrust faults: a discrete-element study. Marine and Petroleum Geology 24, 75-90.

Hardy, S., 2013. Propagation of blind normal faults to the surface in basaltic sequences: Insights from 2D discrete element modelling. Marine and Petroleum Geology 48, 149-159.

Haug, Ø., Galland, O., Souloumiac, P., Souche, A., Guldstrand, F., Schmiedel, T., Maillot, B., 2018. Shear Versus Tensile Failure Mechanisms Induced by Sill Intrusions: Implications for Emplacement of Conical and Saucer-Shaped Intrusions. Journal of Geophysical Research: Solid Earth 123, 3430-3449.

Hubbard, S.M., Romans, B.W., Graham, S.A., 2007. An outcrop example of large-scale conglomeratic intrusions sourced from deep-water channel deposits, Cerro Toro Formation, Magallanes basin, southern Chile. AAPG Memoir 87, 199-207.

Hughes, A.N., Benesh, N.P., Shaw, J.H., 2014. Factors that control the development of fault-bend versus fault-propagation folds: Insights from mechanical models based on the discrete element method (DEM). Journal of Structural Geology 68, 121-141.

Hurst, A., Cartwright, J., Duranti, D., 2003a. Fluidization structures produced by upward injection of sand through a sealing lithology. Geological Society, London, Special Publications 216, 123-138.

Hurst, A., Cartwright, J., Huuse, M., Jonk, R., Schwab, A., Duranti, D., Cronin, B., 2003b. Significance of large-scale sand injectites as long-term fluid conduits: evidence from seismic data. Geofluids 3, 263-274.

Hurst, A., Cartwright, J.A., Huuse, M., Duranti, D., 2006. Extrusive sandstones (extrudites): A new class of stratigraphic trap? Geological Society, London, Special Publications 254, 289-300.

Hurst, A., Cartwright, J., 2007. Relevance of sand injectites to hydrocarbon exploration and production. AAPG Memoir 87, 1-19.

Hurst, A., Scott, A., Vigorito, M., 2011. Physical characteristics of sand injectites. Earth-Science Reviews 106, 215-246.

Hurst, A., Huuse, M., Duranti, D., Vigorito, M., Jameson, E., Schwab, A., 2016. Application of outcrop analogues in successful exploration of a sand injection complex, Volund Field, Norwegian North Sea. Geological Society, London, Special Publications 436, 75-92.

Hurst, A., Vigorito, M., 2017. Saucer-shaped sandstone intrusions: An underplayed reservoir target. AAPG Bulletin 101, 625-633.

Huuse, M., Duranti, D., Guargena, C.G., Prat, P., Holm, K., Steinsland, N., Cronin, B.T., Hurst, N., 2003. Sandstone intrusions: Detection and significance for exploration and production. First Break 21, 15-24.

Huuse, M., Duranti, D., Steinsland, N., Guargena, C.G., Prat, P., Holm, K., Cartwright, J.A., Hurst, A., 2004. Seismic characteristics of large-scale sandstone intrusions in the Paleogene of the south Viking Graben, UK and Norwegian North Sea. Geological Society, London, Memoirs 29, 263-278.

Huuse, M., Mickelson, M., 2004. Eocene sandstone intrusions in the Tampen Spur area (Norwegian North Sea Quad 34) imaged by 3D seismic data. Marine and Petroleum Geology 21, 141-155.

Huuse, M., Shoulders, S.J., Netoff, D.I., Cartwright, J., 2005a. Giant sandstone pipes record basin-scale liquefaction of buried dune sands in the Middle Jurassic of SE Utah. Terra Nova 17, 80-85.

Huuse, M., Cartwright, J.A., Gras, R., Hurst, A., 2005b. Kilometre-scale sandstone intrusions in the Eocene of the Outer Moray Firth (UK North Sea): migration paths, reservoirs and potential drilling hazards. Petroleum Geology: North-West Europe and Global Perspectives—Proceedings of the 6th Petroleum Geology Conference, 1577–1594.

Huuse, M., Cartwright, J., Hurst, A., Steinsland, N., 2007. Seismic characterization of large-scale sandstone intrusions. Geological Society, London, Memoirs, 29, 263-278.

Huuse, M., Jackson, C.A.L., Van Rensbergen, P., Davies, R.J., Flemings, P.B., Dixon, R.J., 2010. Subsurface sediment remobilization and fluid flow in sedimentary basins: an overview. Basin Research 22, 342-360.

Itasca, 2004. Particle Flow Code in 2-Dimensions (PFC2D) manual version 3.10. Minneapolis, Minnesota.

Jackson, C.A.L., Hurst, A., Cartwright, J.A., 2007. The geometry, distribution and development of clastic injectites in deep-marine depositional systems: Examples from the Late Cretaceous Kyrre Formation, Måløy slope, Norwegian margin. Sand injectites: Implications for hydrocarbon exploration and production: AAPG Memoir 87, 37-48.

Jackson, C.A.L., Huuse, M., Barber, G.P., 2011. Geometry of winglike clastic intrusions adjacent to a deep-water channel complex: Implications for hydrocarbon exploration and production. AAPG Bulletin 95, 559-584.

Jackson, C.A.L., Sømme, T.O., 2011. Borehole evidence for wing-like clastic intrusion complexes on the western Norwegian margin. Journal of the Geological Society 168, 1075-1078.

Jackson, C.A.L., Schofield, N., Golenkov, B., 2013. Geometry and controls on the development of igneous sill–related forced folds: A 2-D seismic reflection case study from offshore southern Australia. Geological Society of America Bulletin 125, 1874-1890.

Jenkins, O.P., 1930. Sandstone dikes as conduits for oil migration through shales. AAPG Bulletin 14, 411-421.

Jolly, R.J.H., Lonergan, L., 2002. Mechanisms and controls on the formation of sand intrusions. Journal of the Geological Society 159, 605-617.

Kavanagh, J.L., Menand, T., Sparks, R.S.J., 2006. An experimental investigation of sill formation and propagation in layered elastic media. Earth and Planetary Science Letters 245, 799-813.

Liu, Y., Konietzky., H., 2018. Particle-based modelling of pull-apart basin development. Tectonics 37, 343-358.

Løseth, H., Raulline, B., Nygård, A., 2013. Late Cenozoic geological evolution of the northern North Sea: development of a Miocene unconformity reshaped by large-scale Pleistocene sand intrusion. Journal of the Geological Society 170, 133-145.

Lonergan, L., Cartwright, J.A., 1999. Polygonal faults and their influence on deep-water sandstone reservoir geometries, Alba Field, United Kingdom central North Sea. AAPG Bulletin 83, 410-432.

Lonergan, L., Lee, N., Johnson, H.D., Cartwright, J.A., Jolly, R.J.H., 2000. Remobilisation and injection in deepwater depositional systems: Implications for reservoir architecture and prediction. GCSSEPM Foundation 20th Annual Research Conference: Deep-Water Reservoirs of the World, 515-532.

Lonergan, L., Borlandelli, C., Taylor, A., Quine, M., Flanagan, K., 2007. The three-dimensional geometry of sandstone injection complexes in the Gryphon field, United Kingdom North Sea. AAPG Memoir 87, 103-112.

Mathieu, L., De Vries, B.V.W., Holohan, E.P., Troll, V.R., 2008. Dykes, cups, saucers and sills: Analogue experiments on magma intrusion into brittle rocks. Earth and Planetary Science Letters 271, 1-13.

Menand, T., 2008. The mechanics and dynamics of sills in layered elastic rocks and their implications for the growth of laccoliths and other igneous complexes. Earth and Planetary Science Letters 267, 93-99.

Meng, Q., Hooker, J., Cartwright, J., 2017. Genesis of natural hydraulic fractures as an indicator of basin inversion. Journal of Structural Geology 102, 1-20.

Meng, Q., Hodgetts, D., 2019. Combined control of décollement layer thickness and cover rock cohesion on structural styles and evolution of fold belts: A discrete element modelling study. Tectonophysics, https://doi.org/10.1016/j.tecto.2019.03.004.

Molyneux, S., Cartwright, J.A., Lonergan, L., 2002. Conical amplitude anomalies as evidence for large scale sediment intrusions. First Break 20, 123-129.

Moreau, J., Ghienne, J.F., Hurst, A., 2012. Kilometre-scale sand injectites in the intracratonic Murzuq Basin (South-west Libya): an igneous trigger? Sedimentology 59, 1321-1344.

Mourgues, R., Bureau, D., Bodet, L., Gay, A., Gressier, J.B., 2012. Formation of conical fractures in sedimentary basins: Experiments involving pore fluids and implications for sandstone intrusion mechanisms. Earth and Planetary Science Letters 313, 67-78.

Nichols, R.J., 1995. The liquification and remobilization of sandy sediments. Geological Society, London, Special Publications 94, 63-76.

Omosanya, K.O., Johansen, S.E., Eruteya, O.E., Waldmann, N., 2017. Forced folding and complex overburden deformation associated with magmatic intrusion in the Vøring Basin, offshore Norway. Tectonophysics 706, 14-34.

Palladino, G., Grippa, A., Bureau, D., Alsop, G.I., Hurst, A., 2016. Emplacement of sandstone intrusions during contractional tectonics. Journal of Structural Geology 89, 230-249.

Palladino, G., Alsop, G.I., Grippa, A., Zvirtes, G., Phillip, R.P., Hurst, A., 2018. Sandstone-filled normal faults: A case study from central California. Journal of Structural Geology, 110, 86-101.

Peterson, G.L., 1966. Structural interpretation of sandstone dikes, northwest Sacramento Valley, California. Geological Society of America Bulletin 77, 833-842.

Pollard, D.D., Johnson, A.M., 1973. Mechanics of growth of some laccolithic intrusions in the Henry Mountains, Utah, II: bending and failure of overburden layers and sill formation. Tectonophysics 18, 311-354.

Rodrigues, N., Cobbold, P.R., Løseth, H., 2009. Physical modelling of sand injectites. Tectonophysics 474, 610-632.

Schöpfer, M.P.J., Childs, C., Walsh, J.J., 2006. Localisation of normal faults in multilayer sequences. Journal of Structural Geology 28, 816-833.

Schöpfer, M.P.J., Childs, C., Walsh, J.J., 2007. Two-dimensional distinct element modeling of the structure and growth of normal faults in multilayer sequences: 1. Model calibration, boundary conditions, and selected results. Journal of Geophysical Research: Solid Earth 112, B10401, doi:10.1029/2006JB00490.

Schöpfer, M.P.J., Arslan, A., Walsh, J.J., Childs, C., 2011. Reconciliation of contrasting theories for fracture spacing in layered rocks. Journal of Structural Geology 33, 551-565.

Schöpfer, M.P.J., Childs, C., Walsh, J.J., Manzocchi, T., 2016. Evolution of the internal structure of fault zones in three-dimensional numerical models of normal faults. Tectonophysics 666, 158-163.

Schöpfer, M.P.J., Childs, C., Manzocchi, T., Walsh, J.J., 2017. Three-dimensional distinct element method modelling of the growth of normal faults in layered sequences. Geological Society, London, Special Publications 439, 307-332.

Schmiedel, T., Galland, O., Breitkreuz, C., 2017. Dynamics of sill and laccolith emplacement in the brittle crust: Role of host rock strength and deformation mode. Journal of Geophysical Research: Solid Earth 122, 8860-8871.

Scott, A., Hurst, A., Vigorito, M., 2013. Outcrop-based reservoir characterization of a kilometer-scale sand-injectite complex. AAPG Bulletin 97, 309-343.

Shoulders, S.J., Cartwright, J., 2004. Constraining the depth and timing of large-scale conical sandstone intrusions. Geology 32, 661-664.

Shoulders, S.J., Cartwright, J., Huuse, M., 2007. Large-scale conical sandstone intrusions and polygonal fault systems in Tranche 6, Faroe-Shetland Basin. Marine and Petroleum Geology 24, 173-188.

Spence, G.H., Finch, E., 2014. Influences of nodular chert rhythmites on natural fracture networks in carbonates: an outcrop and two-dimensional discrete element modelling study. Geological Society, London, Special Publications 374, SP374-318.

Szarawarska, E., Huuse, M., Hurst, A., De Boer, W., Lu, L., Molyneux, S., Rawlinson, P., 2010. Three-dimensional seismic characterisation of large-scale sandstone intrusions in the lower Palaeogene of the North Sea: completely injected vs. in situ remobilised sandbodies. Basin Research 22, 517-532.

Vétel, W., Cartwright, J., 2010. Emplacement mechanics of sandstone intrusions: insights from the Panoche Giant Injection Complex, California. Basin Research 22, 783-807.

Vidal-Royo, O., Hardy, S., Muñoz, J.A., 2011. The roles of complex mechanical stratigraphy and syn-kinematic sedimentation in fold development: insights from discrete-element modelling and application to the Pico del Águila anticline (External Sierras, Southern Pyrenees). Geological Society, London, Special Publications 349, 45-60.

Vigorito, M., Hurst, A., Cartwright, J., Scott, A., 2008. Regional-scale subsurface sand remobilization: geometry and architecture. Journal of the Geological Society 165, 609-612.

Virgo, S., Abe, S., Urai, J.L., 2013. Extension fracture propagation in rocks with veins: Insight into the crack-seal process using Discrete Element Method modeling. Journal of Geophysical Research: Solid Earth 118, 5236-5251.

Virgo, S., Abe, S., Urai, J.L., 2014. The evolution of crack seal vein and fracture networks in an evolving stress field: Insights from Discrete Element Models of fracture sealing. Journal of Geophysical Research: Solid Earth 119, 8708-8727.

Virgo, S., Abe, S., Urai, J.L., 2016. The influence of loading conditions on fracture initiation, propagation, and interaction in rocks with veins: Results from a comparative Discrete Element Method study. Journal of Geophysical Research: Solid Earth 121, 1730-1738.

Weertman, J., 1980. The stopping of a rising, liquid-filled crack in the Earth's crust by a freely slipping horizontal joint. Journal of Geophysical Research: Solid Earth 85, 967-976.

**Figure captions**

Fig. 1. Schematic diagrams illustrating the changed channel geometries after sand remobilisation. Note the domal or irregular surface of remolilised channels. Modified from (Lonergan et al., 2000).

Fig. 2. (a) Geometry and boundary conditions of the discrete element models. The enlarged area shows particle contacts. (b) Two particles bounded by a normal and shear spring.

Fig. 3. Modelling results of models 1-4 with a relatively thin overburden. The bonding cohesion increases from 1 to 4 MPa from model 1 to 4. Dashed lines represent fault traces. Arrows indicate relative displacement.

Fig. 4. Modelling results of models 5-10 with an intermediate-thickness overburden. The bonding cohesion increases from 1 to 6 MPa from model 5 to 10. The enlarged boxes show detailed features of opening voids and fractures. Dashed lines represent fault traces. Arrows indicate relative displacement.

Fig. 5. Modelling results of models 11-18 with a relatively thick overburden. The bonding cohesion increases from 1 to 8 MPa from model 11 to 18. The enlarged boxes show detailed features of opening voids and fractures. Dashed lines represent fault traces. Arrows indicate relative displacement.

Fig. 6. Evolving deformation patterns (a) and stress fields (b) of model 5 during incremental sand injections. A number of 463, 1221, 2281, 3571, 5087 and 6863 particles were injected into the overlying layers at T1 to T6.

Fig. 7. Evolving deformation patterns (a) and stress fields (b) of model 14 during incremental sand injections. A number of 276, 1060, 2214, 3633, 5091 and 6751 particles were injected into the overlying layers at T1 to T6.

Fig. 8. Plot of cove rock cohesion versus structural relief of the surface ‘h’ versus width of uplifted area ‘*w*’ of the 18 discrete element models. See the illustration of measurement of *h* and *w* in Fig. 3d.

Fig. 9. Seismic profiles showing characteristics of remobilised channel sands and normal fault systems developed in the overlying sediments. Note that the upper marker horizons were not uplifted. (a) Five normal faults developed in sediments above a channel with an irregular surface. Modified from (Jackson, 2007). Note the domes that uplifted the sediments on the footwall of F2. (b) Three normal faults developed above a remobilised channel. Modified from (Jackson et al., 2011). Note that faulting did not occur in the outer zones of the overlying sediments.

Fig. 10. Field photography and its line drawing showing remobilised channel sands in the Triassic red marls of the Merica Mudstone Group, Somerset, UK. Note the inclined sand wing with a downward tapering tip.

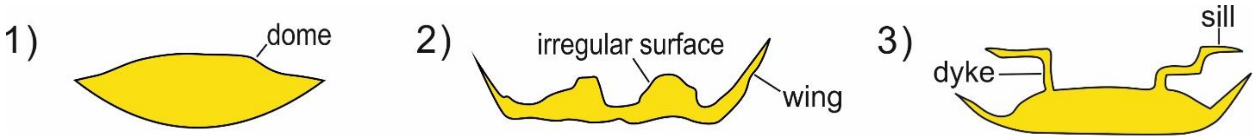


Fig. 1

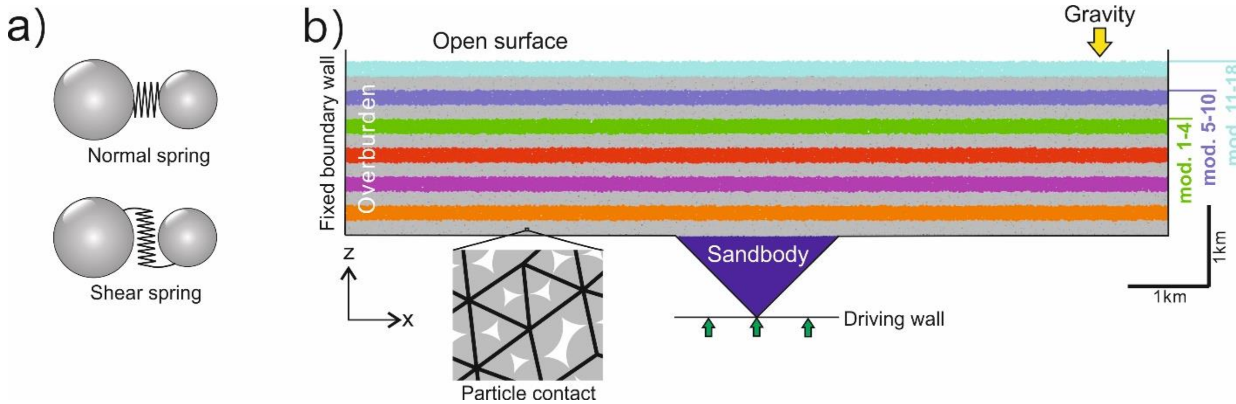

a)
Normal spring
Shear spring
b)
Open surface
Gravity
Fixed boundary wall
Overburden
mod. 1-4
mod. 5-10
mod. 11-18
1km
1km
z
x
Sandbody
Driving wall
Particle contact


Fig. 2

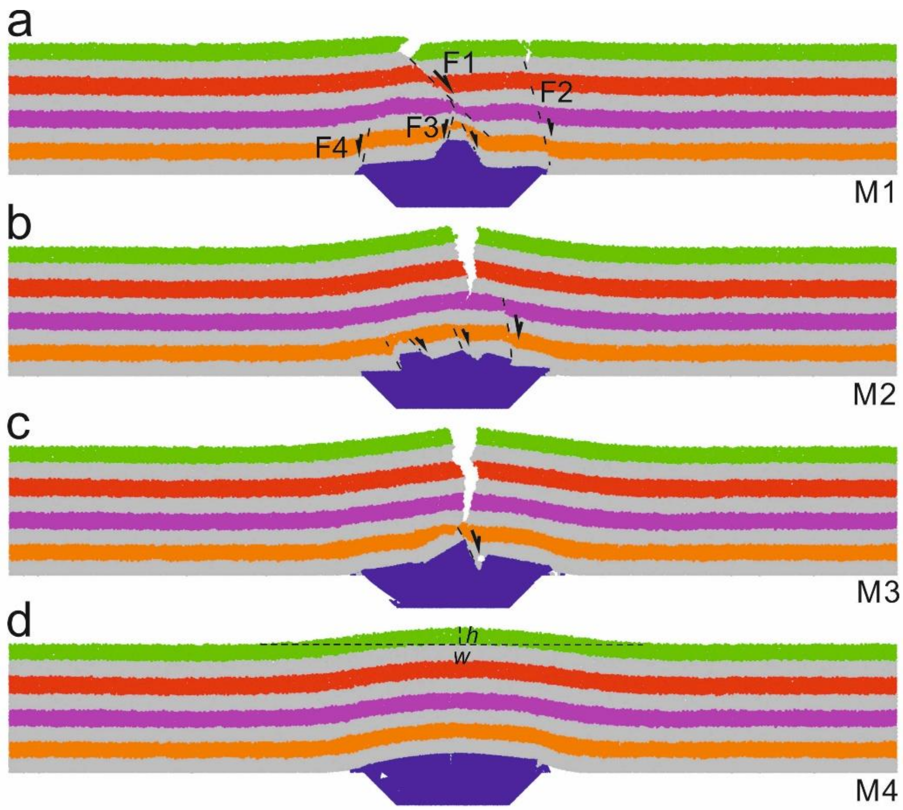


Fig. 3

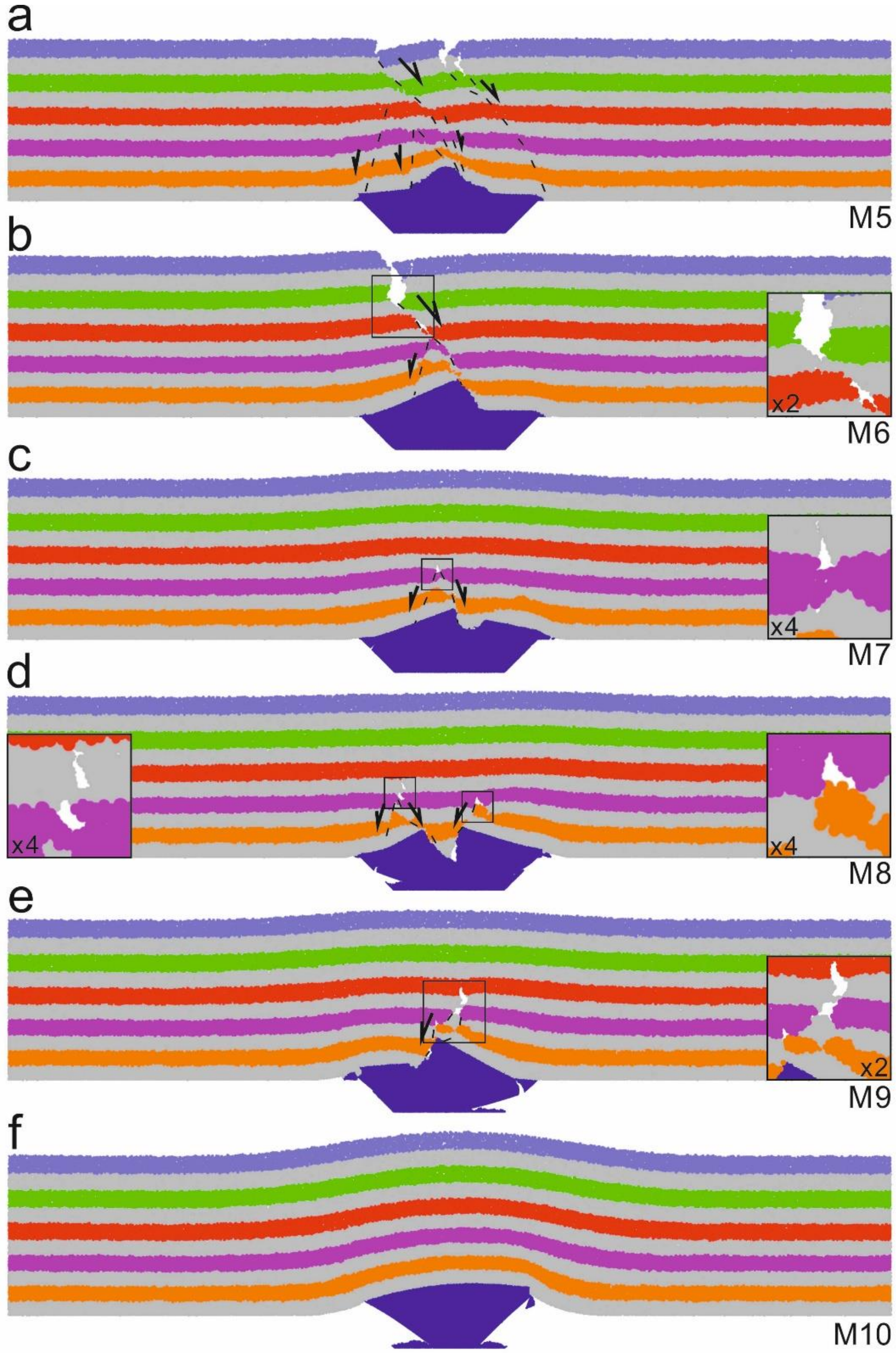


Fig. 4

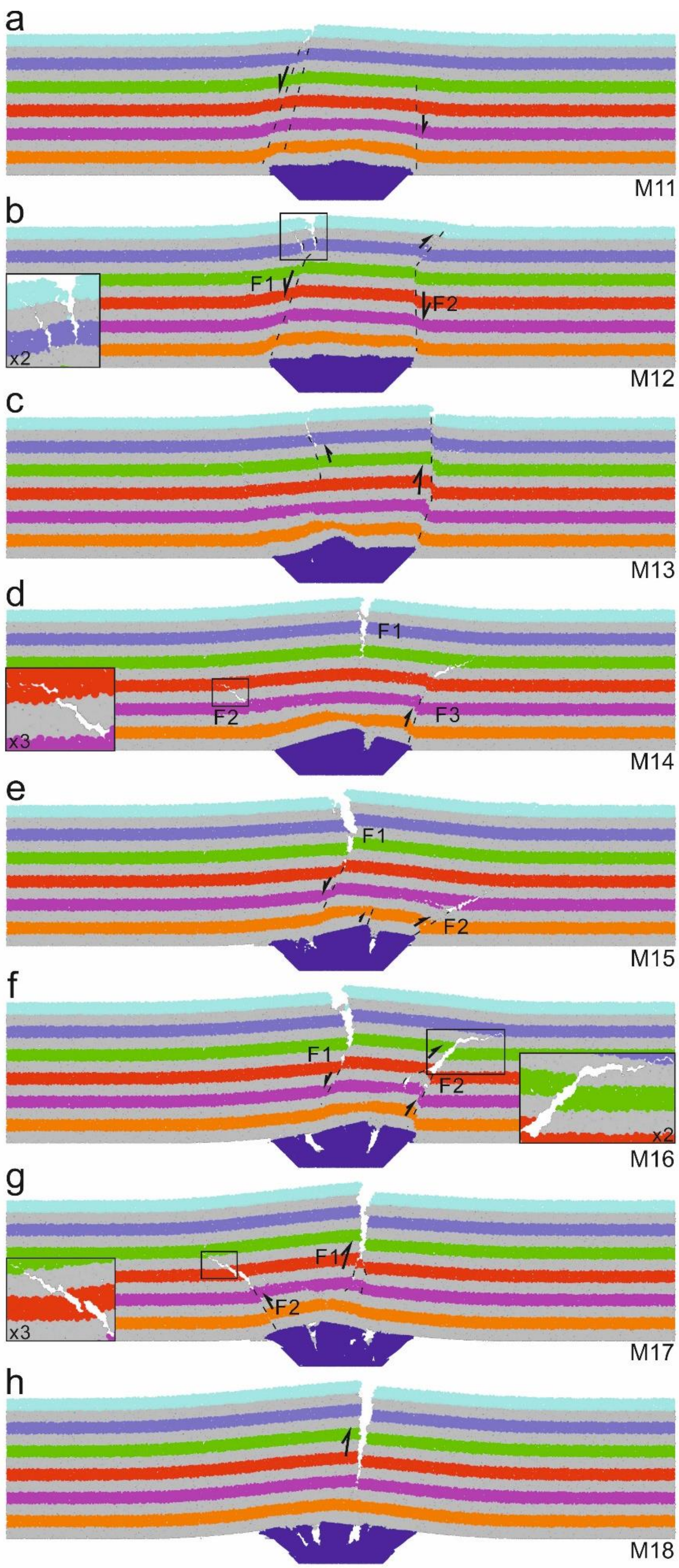
a
M11
b
F1
F2
x2
M12
c
M13
d
F1
F2
F3
x3
M14
e
F1
F2
M15
f
F1
F2
x2
M16
g
F1
F2
x3
M17
h
M18

Fig. 5

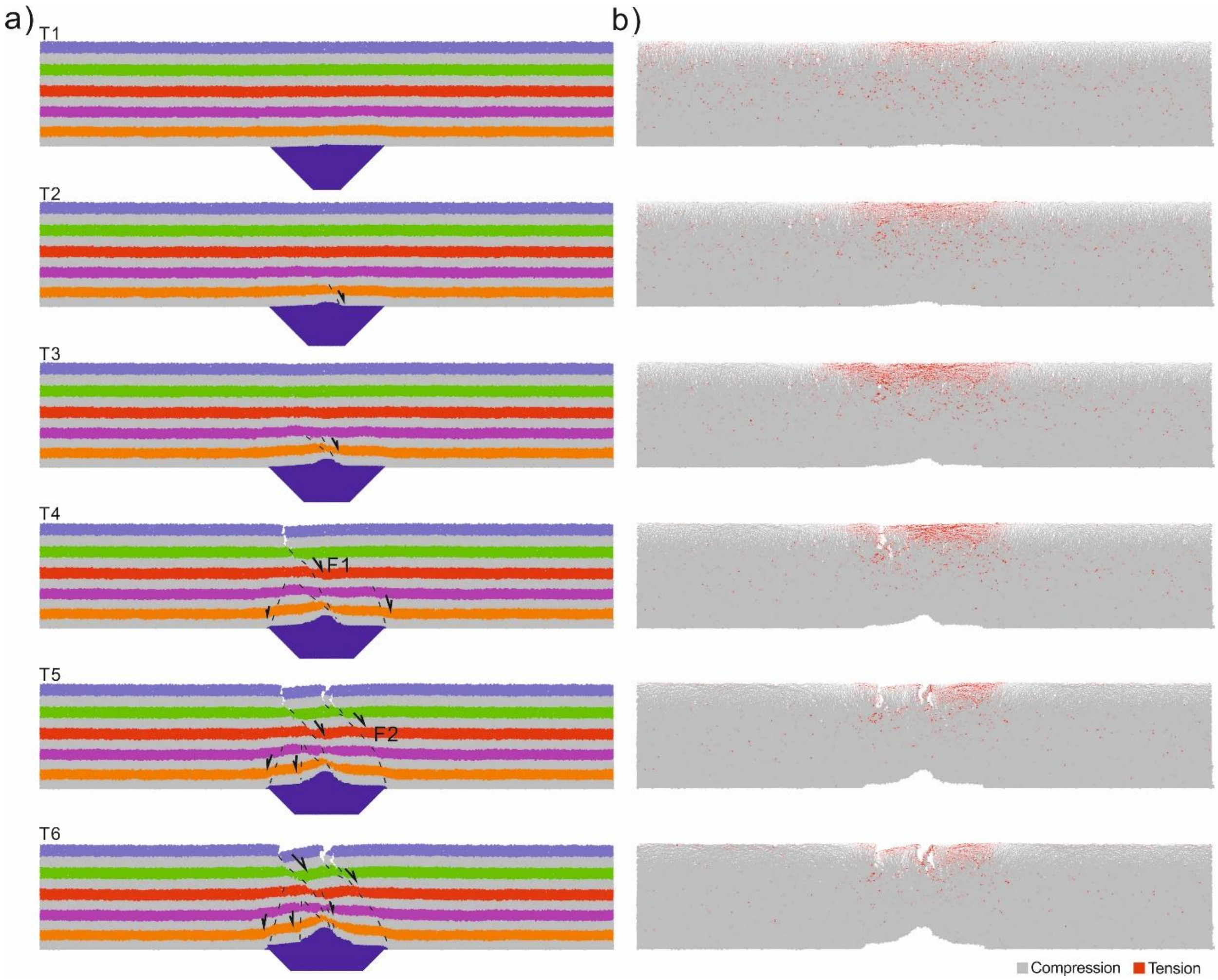


Fig. 6

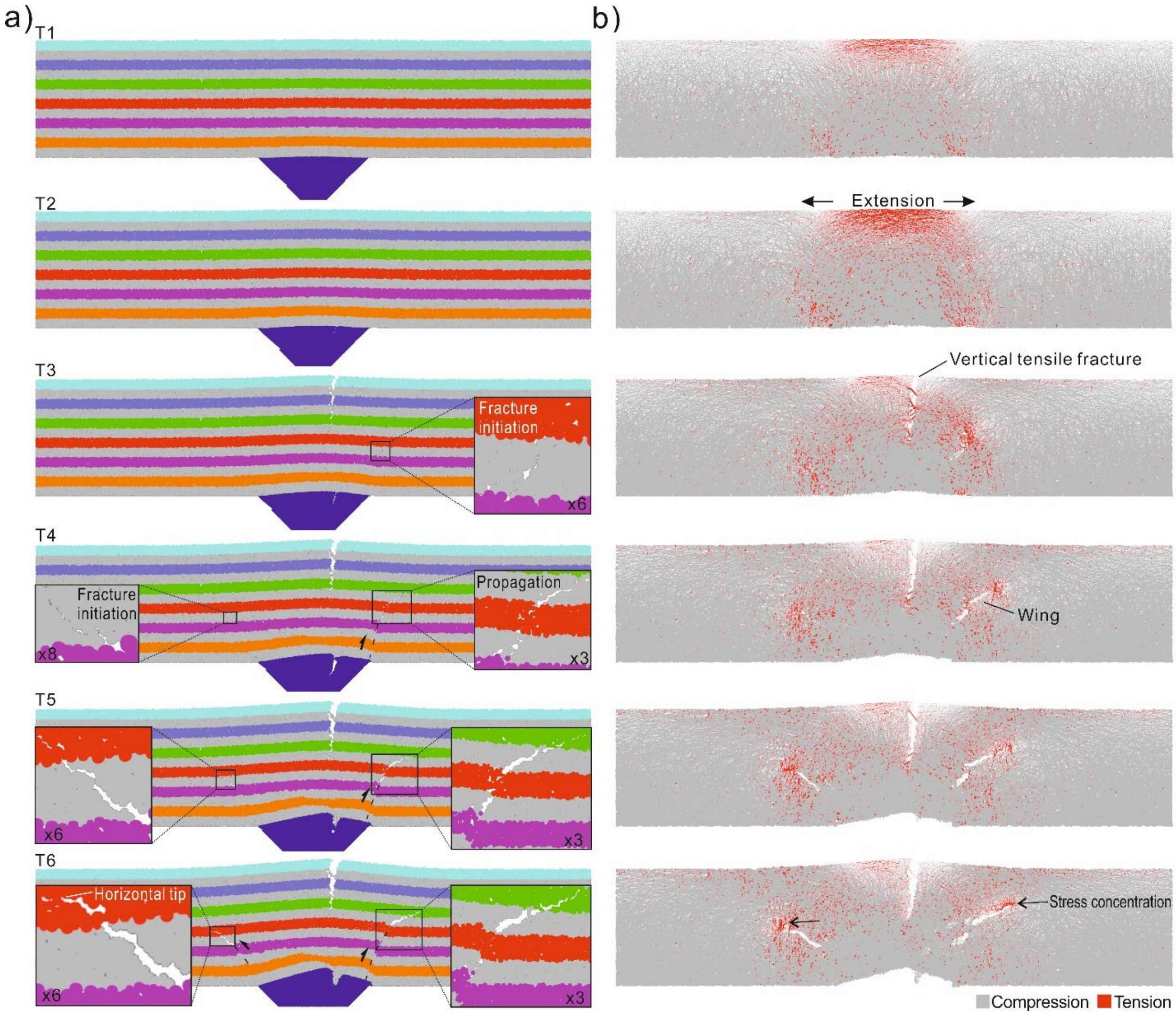
a)
T1
T2
T3
Fracture initiation
x6
T4
Fracture initiation
x8
Propagation
x3
T5
x6
x3
T6
Horizontal tip
x6
x3
b)
Extension
Vertical tensile fracture
Wing
Stress concentration
Compression
Tension

Fig. 7

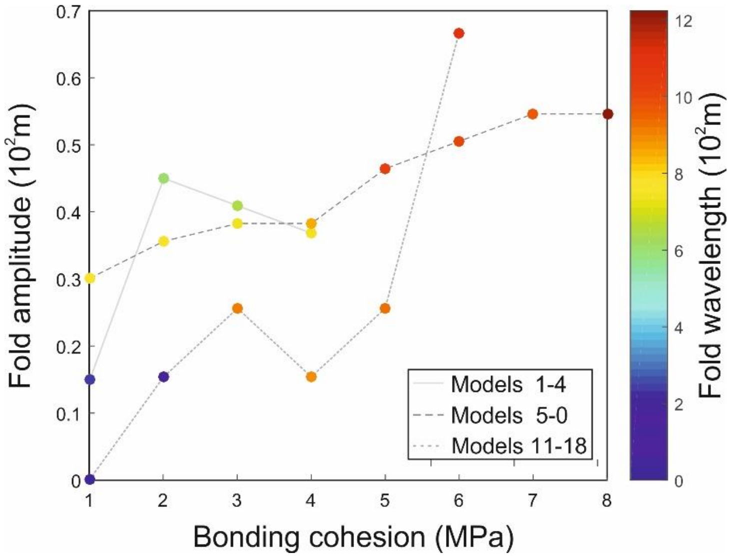

Fold amplitude (10$^2$m)
0
0.1
0.2
0.3
0.4
0.5
0.6
0.7
1
2
3
4
5
6
7
8
Bonding cohesion (MPa)
Fold wavelength (10$^2$m)
0
2
4
6
8
10
12
Models 1-4
Models 5-0
Models 11-18


Fig. 8

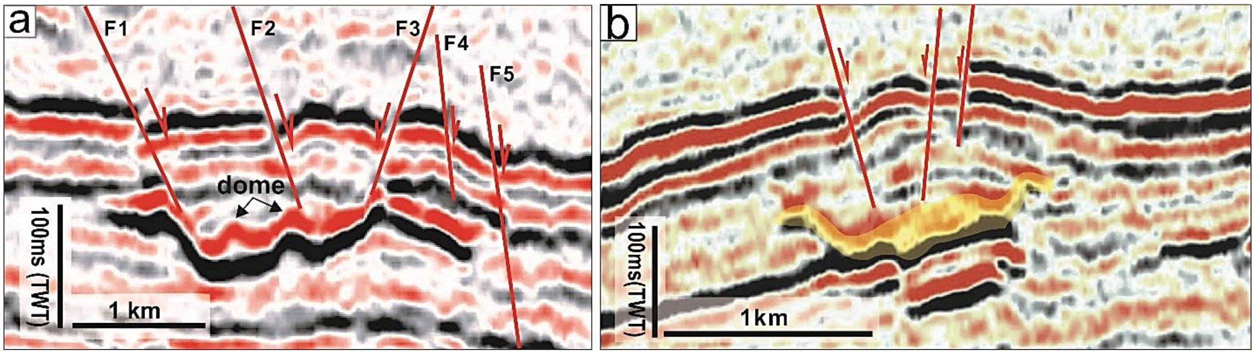


Fig. 9

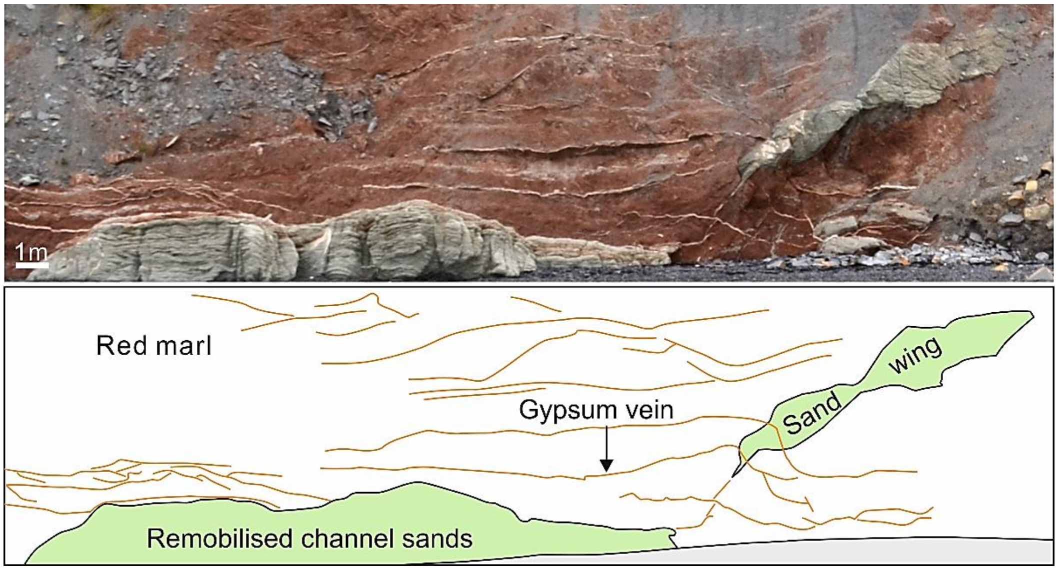
1m
Red marl
Gypsum vein
Sand
wing
Remobilised channel sands

Fig. 10